Bond-length distribution in tetrahedral versus octahedral semiconductor alloys: The case of $Ga_{1-x}In_xN$

L. Bellaiche, S.-H. Wei, and Alex Zunger
National Renewable Energy Laboratory, Golden, Colorado 80401
(Received 27 May 1997)

Large ($\approx$1000 atoms) supercell valence force-field simulations are used to investigate the nearest-neighbor bond-length distribution in relaxed tetrahedral (zinc blende and wurtzite) and octahedral (rocksalt) $Ga_{1-x}In_xN$ alloys. We find that, due to the rigidity of the octahedron, the distribution of each anion-cation bond length in *rocksalt alloys* has two contributions: unrelaxed bonds and relaxed bonds. These two peaks have a large width and overlap slightly, leading to a broad nearest-neighbor distance distribution. On the other hand, the anion-cation nearest-neighbor distribution in *zinc-blende alloys* can be decomposed into a sum over four closely spaced and sharp peaks associated with different clusters, leading to a narrow, single-peaked nearest-neighbor distribution. Finally the wurtzite alloys exhibit bond-length distributions that are very similar to the corresponding ones in the zinc-blende alloys, leading to a nearly identical strain energy in random zinc-blende and wurtzite alloys. [S0163-1829(97)04045-9]

I. INTRODUCTION

When an $A_{1-x}B_xC$ alloy is formed from lattice mismatched constituents AC and BC, its lattice constant $a(x)$ tends to be close to the composition-weighted average values (Vegard's rule), but the individual bond lengths $R_{AC}(x)$ and $R_{BC}(x)$ remain distinct.[1,2] This tendency has been studied extensively for *zinc-blende alloys*, and is now well understood in terms of atomistic relaxation models.[2–11] In these models, atoms are displaced from their lattice sites so as to minimize the strain energy that results from the difference between the actual bond lengths R_{AC} and R_{BC} and the ideal bond lengths R^0_{AC} and R^0_{BC}, as well as from the difference between the actual bond angles Θ and the ideal (e.g., tetrahedral) bond angle Θ^0. Due to the topological frustration of common crystal configurations,[12] a complete relaxation to reach *both* ideal bond lengths and ideal bond angles is usually not possible. In fact, there are only two ordered adamantine structures, where diamondlike constituents can attain the ideal bond configurations—the zinc-blende structure and the RH1 structure.[12] Thus, in general, the alloy system relaxes into a ''compromise structure,'' exhibiting a *distribution* of bond lengths and angles around the ideal values. Experimental measurements[1,2] show that zinc-blende alloys exhibit bimodal anion-cation bond-length distribution, with only one type of A-C bond and only one type of B-C bond. Furthermore, experiment shows that with respect to the bond lengths R^0_{AC} and R^0_{BC} of the end-point constituents, if $R^0_{BC} \geqslant R^0_{AC}$ then $R_{AC}(x) \geqslant R^0_{AC}$ and $R_{BC}(x) \leqslant R^0_{BC}$.

In this paper we investigate the magnitude and distribution of bond lengths in *rocksalt* and *wurtzite* alloys and compare them with the corresponding quantities in zinc-blende alloys. Our interest in rocksalt alloys stems both from recent measurements on such systems,[13–16] and from an interesting geometric difference between a tetrahedral alloy and an octahedral alloy that could have a consequence on bond-length distribution. To see this difference, note that when A and B atoms (''mixed sublattice'') are located at their lattice sites, the nearest-neighbor A-C and B-C bonds in an octahedral alloy are all parallel or perpendicular to the octahedral axis. Displacement of a C atom from the center of the octahedron towards a given vertex occupied by say, an A atom, shortens that bond, but, to first order, does not change the length of the other *perpendicular* bonds which remain ''unrelaxed.'' Thus, this ''rigidity'' of the octahedral alloy could lead to two types of A-C bonds: ''relaxed'' and ''unrelaxed.'' On the other hand, the tetrahedral lattice is more ''flexible'' in that a shift of the tetrahedron-centered C atom towards a vertex leads to a change of *all* of the nearest-neighbor tetrahedral bond lengths. This simple geometric difference could have significant effects on the bond-length distributions between an octahedral alloy and a tetrahedral alloy. Indeed we find that (i) the bond-length distribution in rocksalt alloys can be decomposed into two peaks for A-C bonds and two peaks for B-C bonds. These two peaks overlap slightly, leading to a broad A-C (B-C) anion-cation nearest-neighbor distribution, while (ii) the A-C (B-C) bond-length distribution in zinc-blende alloys can be decomposed into a sum over four closely spaced sharp peaks, leading to a single-peaked A-C (B-C) anion-cation nearest-neighbor distribution.

Our interest in the bond-length distribution of *wurtzite* alloys is based on the following consideration: If the bond-length distribution in wurtzite alloys is significantly different from that of zinc-blende alloys, the corresponding strain energies would differ too. In extreme cases, this difference could reverse the order of stability of zinc blende vs wurtzite in the alloy relative to pure constituents. Indeed, in a recent calculation, Van Schilfgaarde, Sher, and Chen[17] find that zinc blende $Ga_{1-x}In_xN$ alloys have a significantly lower formation energy than the corresponding wurtzite alloys, despite the fact that the stable ground-state structure of the pure constituents (GaN and InN) is wurtzite. This intriguing finding could have an important implication on crystal growth of $Ga_{1-x}In_xN$ alloys. Our calculations suggest, however, that the finding of Ref. 17 reflects the limited size of their supercell, and that using larger supercell leads to a bond-length

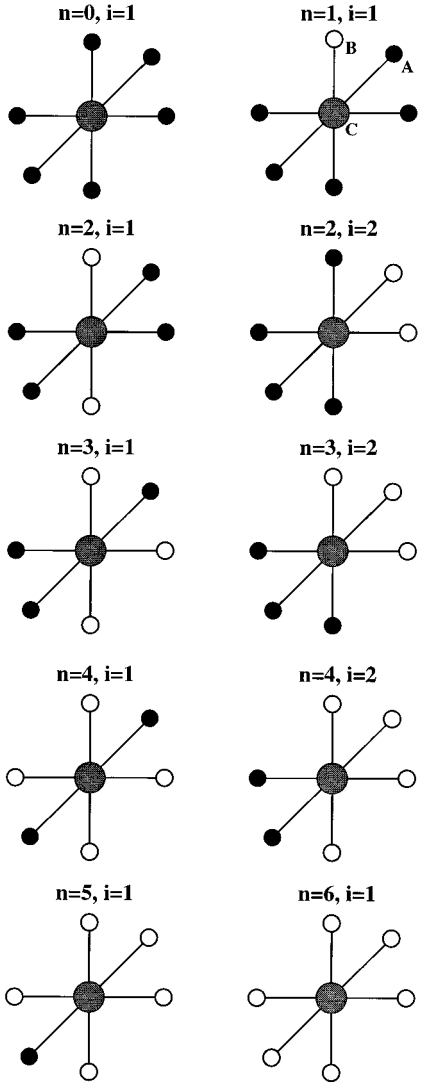

FIG. 1. The 10 symmetry inequivalent geometries (n,i) in a rocksalt $A_{1-x}B_xC$ alloy. i denotes the possible configurations inside $A_{6-n}B_n$ clusters.

distribution and a strain energy nearly identical between zinc-blende and wurtzite alloys. Hence, the ground state of the alloy is the same as that of its constituents.

II. ANALYSIS OF BOND-LENGTH DISTRIBUTION IN OCTAHEDRAL vs TETRAHEDRAL ALLOYS: A SIMPLE MODEL

To shed some light on the problem of bond-length distribution in octahedral vs tetrahedral alloys, we first simplify the problem so that an analytical solution can be obtained. In this simple model, we restrict the atoms A and B of $A_{1-x}B_xC$ to be positioned at their fcc sites and allow only the C atoms to relax to their minimal energy positions. We minimize the strain energy which is assumed to be proportional to $[R_{AC}(x)-R^0_{AC}]^2$ and $[R_{BC}(x)-R^0_{BC}]^2$, where $R_{AC}(x)$ $[R_{BC}(x)]$ is the A-C (B-C) bond lengths at composition x, and R^0_{AC} (R^0_{BC}) is the ''ideal'' bond length in pure AC (BC). We neglect bond bending. A similar model was assumed by Shih *et al.* in Ref. 4 to predict the bond-length

TABLE I. Probabilities of finding different octahedral clusters and bonds in a rocksalt $A_{1-x}B_xC$ alloy [see Eq. (2) and text for complete definition]. The 10 different clusters are shown in Fig. 1.

Cluster	(n,i)	$p(n,i)$	$\omega_{BC}(n,i,j=1)$	$\omega_{BC}(n,i,j=2)$
A_6B_0	(0,1)	1	0	0
A_5B_1	(1,1)	1	0	1/6
A_4B_2	(2,1)	1/5	2/6	0
A_4B_2	(2,2)	4/5	0	2/6
A_3B_3	(3,1)	3/5	2/6	1/6
A_3B_3	(3,2)	2/5	0	3/6
A_2B_4	(4,1)	1/5	4/6	0
A_2B_4	(4,2)	4/5	2/6	2/6
A_1B_5	(5,1)	1	4/6	1/6
A_0B_6	(6,1)	1	6/6	0

relaxations at the dilute limits of octahedral and tetrahedral alloys. In Sec. IV B, we will present a simulation that permits A, B, as well as C atoms to relax simultaneously, and includes bond bending.

The M-fold coordinated alloys ($M=6$ for octahedral alloy, and $M=4$ for tetrahedral alloy) can be decomposed into C-atom centered $A_{M-n}B_n$ clusters ($0\leqslant n\leqslant M$). For random alloy the probability $P^{(n)}_M(x)$ of finding $A_{M-n}B_n$ cluster is equal to

$$P^{(n)}_M(x)=\binom{M}{n}x^n(1-x)^{M-n}. \tag{1}$$

There are also two other probabilities to consider: the probability $p(n,i)$ of finding symmetry inequivalent configurations i in the $A_{M-n}B_n$ cluster, and the probability $\omega_{BC}(n,i,j)$ of finding a jth-type B-C bond R^j_{BC} in configuration i in the $A_{M-n}B_n$ cluster. The total probability of finding $R^j_{BC}(x)$ in an alloy with composition x is then given by

$$P^j_{BC}(x)=\sum_{n,i}\binom{M}{n}x^n(1-x)^{M-n}p(n,i)\omega_{BC}(n,i,j). \tag{2}$$

A similar expression holds for A-C bonds.

A. Octahedral alloys

In octahedral alloys, the bonds are either parallel or perpendicular to each other. To first order in the changes in the bond length due to the displacement of the octahedron-centered C atom, there are only two types of B-C bonds: $j=1$, where the bond is unrelaxed, and $j=2$, where the bond is relaxed. They are equal to

$$R^{j=1}_{BC}(x)=a(x)/2,$$

$$R^{j=2}_{BC}(x)=\frac{a(x)}{2}\left(1+\frac{R^0_{BC}-R^0_{AC}}{a(x)}\right). \tag{3}$$

There are ten symmetry-inequivalent $A_{6-n}B_n$ clusters ($0\leqslant n\leqslant 6$) in octahedral alloys, as shown in Fig. 1. Their probabilities $p(n,i)$ and $\omega_{BC}(n,i,j)$ are given in Table I. Equation (2) (with $M=6$) gives then the following statistical probabilities for finding the two types of bonds of Eq. (3):

$$P^{j=1}_{BC}(x)=x^2,$$

$$P_{BC}^{j=2}(x)=x(1-x). \tag{4}$$

Similarly, for the A-C bonds,

$$R_{AC}^{j=1}(x)=a(x)/2,$$

$$R_{AC}^{j=2}(x)=\frac{a(x)}{2}\left(1-\frac{R_{BC}^0-R_{AC}^0}{a(x)}\right) \tag{5}$$

and

$$P_{AC}^{j=1}(x)=(1-x)^2,$$

$$P_{AC}^{j=2}(x)=x(1-x). \tag{6}$$

Note that at the dilute limits (e.g., a single A atom replacing a B atom in a BC host crystal), the only possible clusters are ($n=5$, $i=1$) or ($n=6$, $i=1$) in Fig. 1. In this dilute limit, $a(x)/2$ is nearly equal to R_{BC}^0, and the AC bond length is determined by Eq. (5) with $j=2$, i.e., $R_{AC}^{j=2}-R_{AC}^0=(R_{BC}^0-R_{AC}^0)/2$. This result was found in Ref. 4 at the dilute impurity limits of rocksalt alloys.

B. Tetrahedral alloys

In tetrahedral alloys, the bonds are not orthogonal to each other. Thus, a displacement of the tetrahedron-centered C atom leads to a bond length change of *all* the nearest-neighbor bonds in the tetrahedron. There are only five symmetry inequivalent clusters $A_{4-n}B_n(0\leqslant n\leqslant 4)$ in tetrahedral alloys, corresponding to the five different possible n. The probabilities have simple expressions: $p(n,i)=1$ and $\omega_{BC}(n,i,j)=j/4$ ($j=n=0$, 1, 2, 3, and 4). This leads to *four types* of B-C bonds with

$$R_{BC}^{j}(x)=\frac{\sqrt{3}}{4}\,a(x)+\frac{4-j}{4}\,(R_{BC}^0-R_{AC}^0),$$

$$P_{BC}^{j}(x)=\binom{4}{j}x^j(1-x)^{4-j}\,\frac{j}{4}. \tag{7}$$

Similarly, for the A-C bonds,

$$R_{AC}^{j}(x)=\frac{\sqrt{3}}{4}\,a(x)-\frac{j}{4}\,(R_{BC}^0-R_{AC}^0),$$

$$P_{AC}^{j}(x)=\binom{4}{j}x^j(1-x)^{4-j}\,\frac{4-j}{4}. \tag{8}$$

Equations (3)–(8) will serve to analyze the trends in the simulated results.

Note that at the dilute limits (e.g., a single A atom replacing a B atom in a BC host crystal), the only possible clusters are $j=4$ or $j=3$. In this dilute limit, $(\sqrt{3}/4)a(x)$ is nearly equal to R_{BC}^0, and the AC bond length is determined by Eq. (8) with $j=3$, i.e., $R_{AC}^{j=3}-R_{AC}^0=(R_{BC}^0-R_{AC}^0)/4$. This result was found in Ref. 4 at the dilute impurity limits of tetrahedral alloys.

III. SIMULATION METHOD

To study the bond distribution in $Ga_{1-x}In_xN$, we have performed simulations using the valence force-field (VFF) model.[18,19] The total energy $E_{\rm VFF}$ is given by

$$E_{\rm VFF}=\sum_i\ \frac{3}{8(R_i^0)^2}\,\alpha_i[\mathbf{R}_i\cdot\mathbf{R}_i-(R_i^0)^2]^2+\sum_{(i,k)}\ \frac{3}{8R_i^0R_k^0}\,\beta_{(i,k)}\times[\mathbf{R}_i\cdot\mathbf{R}_k-R_i^0R_k^0\cos\,\Theta_{(i,k)}^0]^2 \tag{9}$$

where the first sum runs over all the nearest-neighbor bonds $\mathbf{R}_i$ and the second sum runs over all the bond angles formed between $\mathbf{R}_i$ and $\mathbf{R}_k$ *around each atom*. R_i^0 is the equilibrium interatomic distance, $\Theta_{(i,k)}^0$ is the ideal bond angle, α_i and $\beta_{(i,k)}$ are the bond-stretching and the bond-bending force constants, respectively. When fitted to first-principles calculations, the VFF method has been found to be accurate in predicting bond lengths in semiconductor alloys.[8,11] We used the bond-stretching (α) and bond-bending (β) force constants derived from first-principles calculations[20] for GaN ($\alpha=96.30$ N/m and $\beta=14.80$ N/m) and InN ($\alpha=79.20$ N/m and $\beta=14.10$ N/m).[21,22] For rocksalt and zinc-blende alloys, the random alloy is mimicked by a 1024-atom ''special quasirandom structure'' (SQS) for which the fcc-mixed sublattice has the same pair-correlation functions as the random alloy for the first eight neighbor shells. For the wurtzite alloys, we use an 864-atom supercell and randomly occupy the mixed sublattice by Ga and In atoms for a given composition. We also assume that the pure wurtzite compounds have an ideal c/a axial ratio (equal to $\sqrt{8/3}\simeq 1.633$) and an ideal internal parameter u (equal to 0.375), so as to conserve the exact tetrahedral environment. In fact, c/a and u in both wurtzite GaN and wurtzite InN differ only slightly (by less than 1%) from the ideal values,[23] leading to only a small VFF energy difference between the c/a and u relaxed structure and the structure with ideal values. This difference is 0.9 meV/atom for pure GaN and 1.4 meV/atom for pure InN.

The simulations are performed for three different compositions: $x=0.25$, 0.50, and 0.75. For all structures and compositions, the lattice constant is assumed here to vary linearly as a function of the composition x, as actually found for $Ga_{1-x}In_xN$ in first-principles local-density-approximation (LDA) total-energy calculations.[24]

IV. RESULTS AND DISCUSSIONS

A. Unrelaxed cation sublattice: Octahedral vs tetrahedral alloys

We first simulate the random $Ga_{1-x}In_xN$ alloy by fixing the cation positions on the ideal lattice sites, letting only the *common* sublattice (i.e., the anion sublattice in that case) relax. This allows us to compare the results of the simulation with the analytic expectations of Sec. II, which made this assumption.

Figures 2(a)–2(c) show the bond-length distributions for octahedral rocksalt structure for $x=0.25$, 0.50, and 0.75, respectively, while Figs. 2(d)–2(f) show the corresponding results for cation-unrelaxed zinc-blende alloys. As expected from Sec. II, the rocksalt alloys exhibit two peaks for *each* bond (Ga-N or In-N), while the zinc-blende alloys show, in

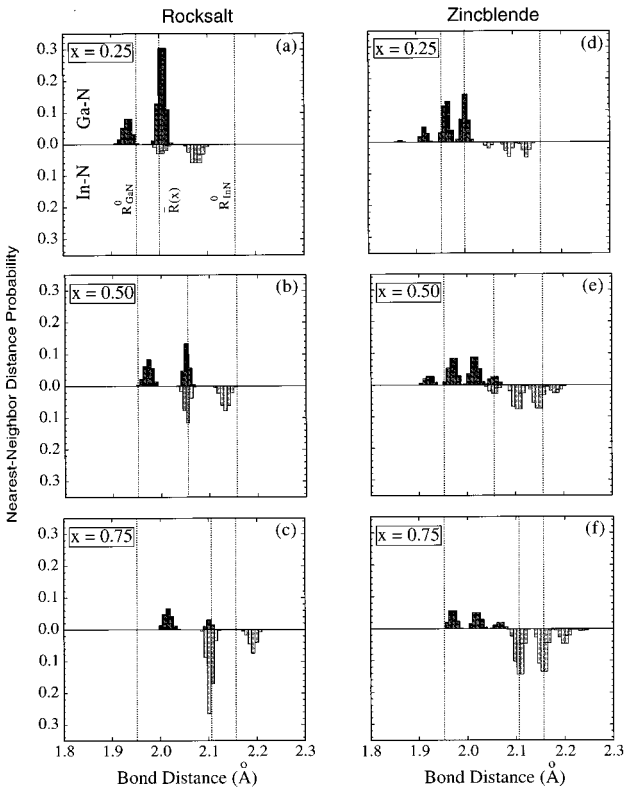

FIG. 2. Histogram of the bond-length distribution in the unrelaxed cation lattice $Ga_{1-x}In_xN$ alloys. (a), (b), and (c) pertain to rocksalt alloys, for $x=0.25$, 0.50, and 0.75, respectively, for which two different peaks can be seen for each cation-anion bond. (d), (e), and (f) concern zinc-blende alloys, for which four distinct peaks exist for each bond. The upper part of each panel corresponds to the Ga-N bond, while the lower part corresponds to the In-N bond. The vertical dashed lines indicate (from left to right) the values of the ideal bond R^0_{GaN}, the composition averaged ''virtual lattice'' bond [equal to $a(x)/2$ in rocksalt alloys and to $\sqrt{3}a(x)/4$ in zinc-blende alloys], and the ideal bond R^0_{InN}, respectively.

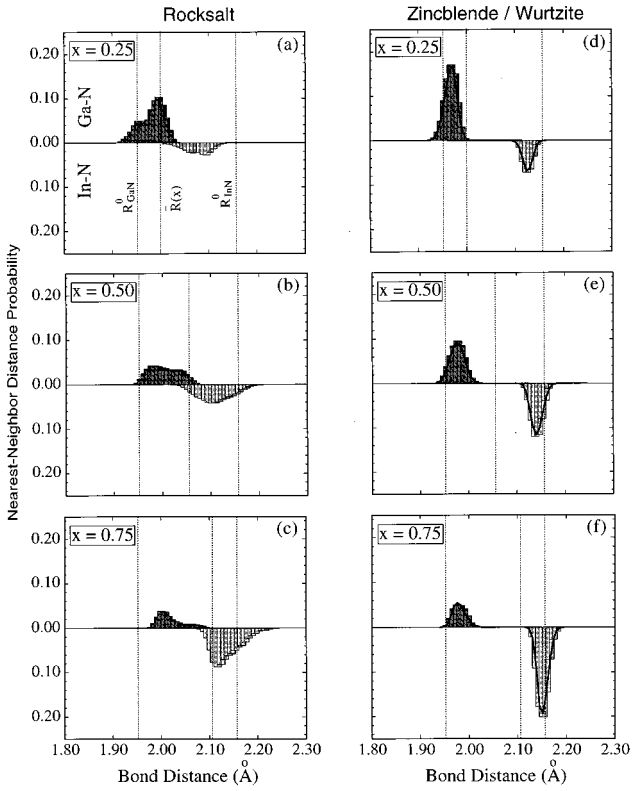

FIG. 3. Histogram of the nearest-neighbor bond-length distribution in the *fully* relaxed $Ga_{1-x}In_xN$ alloys. (a), (b), and (c) pertain to rocksalt alloys, for $x=0.25$, 0.50, and 0.75, respectively. (d), (e), and (f) concern zinc-blende alloys. The results for the wurtzite alloys are also indicated in (d), (e), and (f) by the thick solid lines. The upper part of each panel corresponds to the Ga-N bond, while the lower part corresponds to the In-N bond. The vertical dashed lines indicate from left to right the values of the ideal bond R^0_{GaN}, the composition averaged ''virtual lattice'' bond [equal $a(x)/2$ in rocksalt alloys and $\sqrt{3}a(x)/4$ in zinc-blende alloys], and the ideal bond R^0_{nN}, respectively.

general, four peaks for each bond. For the rocksalt alloys we found that the unrelaxed bond peaks ($j=1$) occur exactly at the position given by Eqs. (3) and (5), while the relaxed bond peaks ($j=2$) occur at a position differing by less than 0.03 Å from its values given by Eqs. (3) and (5). This small discrepancy between the simulated results and the analytical predictions reflects the competition between the bond stretching and bond bending absent in our analytical model. Furthermore, the broadening of the simulation peaks relative to the analytical expectations of a single value for each type of bond length [see Eqs. (3) and (5)] is partly due to this competition and partly due to higher-order terms which are also neglected in the analysis of Sec. II. On the other hand, the integrated peak probabilities of the two types of Ga-N and In-N bonds are *exactly* those given by Eqs. (4) and (6).

For the tetrahedral zinc-blende alloys, the simulated peaks positions differ once again slightly (by less than 0.03 Å) from their simple predictions [Eqs. (7) and (8)], while the integrated probability follows exactly Eqs. (7) and (8).

B. Relaxed cation and anion sublattices: Rocksalt vs zinc blende vs wurtzite

We now study the effect of the cation sublattice relaxations, as well as the anion sublattice relaxations on the bond-length distribution. Figure 3 shows the bond-length distribution in rocksalt and zinc-blende $Ga_{1-x}In_xN$ alloys, for $x=0.25$, 0.50, and 0.75, when all the atoms are allowed to move from their ideal positions. The results for wurtzite structures are also shown in Fig. 3 as solid lines.

As previously noticed,[11] the bond-length distribution for an A-C bond in a zinc-blende $A_{1-x}B_xC$ alloy looks single-peaked when all the atoms are allowed to relax. In fact, by keeping track of the bonds belonging to each peak displayed in Figs. 2(d)–2(f), we find that the Ga-N (In-N) bond-length distribution can be decomposed into the sum over the four peaks mentioned in Sec. II B, also for the cation and anion-relaxed alloys [see Fig. 4(b)]. However, when all the atoms can move, these four peaks are very close to each other (e.g., they differ by 0.02 Å for In-N bonds at $x=0.50$), and have a small width (e.g., around 0.02 Å for In-N bonds at $x=0.50$),

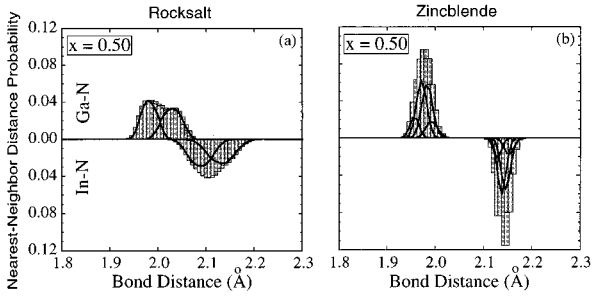

FIG. 4. Decomposition of the histogram of the nearest-neighbor bond-length distribution into a sum over two peaked distributions in the *fully* relaxed $Ga_{0.50}In_{0.50}N$ rocksalt alloys (a) and into a sum over four peaked distributions in the *fully* relaxed $Ga_{0.50}In_{0.50}N$ zinc-blende alloys (b). The upper part of this figure corresponds to the Ga-N bond, while the lower part corresponds to the In-N bond. Each peaked distribution is indicated by means of a thick solid line.

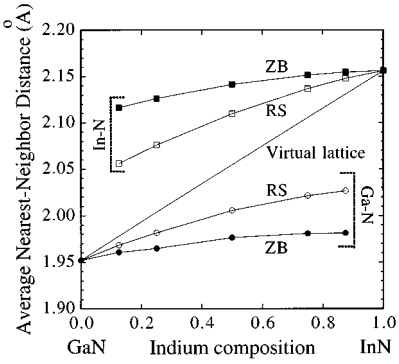

FIG. 5. Dependence of the average nearest-neighbor distance [Eq. (10)] as a function of the indium composition in the fully relaxed rocksalt and zinc-blende $Ga_{1-x}In_xN$ alloys. The open symbols correspond to rocksalt alloys, while the filled symbols correspond to zinc-blende alloys. The circles correspond to the Ga-N bond length, while the squares correspond to the In-N bond length.

leading to a sharp bond-length distribution appearing single-peaked. Furthermore, the integrated intensity is equal to x for the In-N bond, and to $(1-x)$ for the Ga-N bond, as it should be at composition x. We can also define the *weighted average* nearest-neighbor Ga-N bond length as

$$\overline{R}_{\text{Ga-N}}=\frac{1}{m}\sum_i R^i_{\text{Ga-N}}, \tag{10}$$

where the sum runs over the m different Ga-N bonds $R^i_{\text{Ga-N}}$ existing in the histograms displayed in Fig. 2 or 3. A similar definition holds for the *weighted average* nearest-neighbor $R_{\text{In-N}}$ bond length. For each composition, we find that $R_{\text{Ga-N}}$ and $R_{\text{In-N}}$ in cation- and anion-relaxed zinc-blende alloys are almost equal (by less than 0.025 Å) to the corresponding weighted average bond lengths in cation-unrelaxed zinc-blende alloys.

On the other hand, as shown in Figs. 3(a)–3(c) the distributions of the different Ga-N (or In-N) bond lengths in *rocksalt* alloys do not overlap strongly, so in some cases one sees two distinct peaks (see, for example, the Ga-N bonds for $x=0.25$ and 0.75). In fact, we find that, as in the case of cation unrelaxed rocksalt alloys, the bond-length distribution for any composition and for both Ga-N and In-N bonds can be decomposed into the sum over the two different peaked distributions mentioned in Secs. II A and IV A [see Fig. 4(a) for $x=0.5$]. Furthermore, the weighted average nearest-neighbor Ga-N (In-N) distance differs by less than 0.02 Å between fully relaxed and cation-unrelaxed results. However, in the fully relaxed case, the width of the peaks becomes larger (e.g., around 0.07 Å for In-N bonds at $x=0.50$), and the relative positions of the two peaks become closer (e.g., they differ by 0.04 Å for In-N bonds at $x=0.50$) than in the cation-unrelaxed case. This explains the large spread of the nearest-neighbor distance distribution observed in Fig. 3. We also found that these two peaks are more distant and sharper for the short Ga-N bonds than for the longer In-N bonds: for example, at $x=0.50$, the two peaks have a width equal to 0.05 Å and a mutual distance of 0.05 Å for Ga-N bonds, while they have a width of 0.07 Å and a mutual distance around 0.04 Å for In-N bonds. As shown in Fig. 3, it is thus easier to see the two peaks in the distribution of the shortest bonds than in the distribution of the longest bonds. This fact may be consistent with the recent x-ray-absorption fine-structure (XAFS) measurements of Wang and Bunker[16] reporting two distinct Pb-S nearest-neighbor bond lengths, while only finding one single Pb-Te nearest-neighbor bond length in rocksalt $PbS_{1-x}Te_x$ alloys.

As shown in Fig. 5, the weighted average nearest-neighbor bond lengths $R_{\text{Ga-N}}$ and $R_{\text{In-N}}$ are closer to their ideal bulk values in the zinc-blende alloy than in the rocksalt alloy having the same composition. This is due to the fact that the bond relaxation in rocksalt alloys is less complete than in zinc-blende alloys: Fig. 3 shows that in the rocksalt alloys, a significant number of bonds are totally unrelaxed, i.e., they have the composition averaged ''virtual lattice'' bond length [cf. Eqs. (3) and (5) with $j=1$]. This lack of relaxation in rocksalt alloys is consistent with observations of Ref. 14 revealing that the average Rb-Br and Rb-Cl nearest-neighbor distances determined by XAFS are separated by less than 0.05 Å in the $RbBr_{1-x}Cl_x$ alloys, while the nearest-neighbor bond lengths of the two end points RbBr and RbCl differ by about 0.15 Å.

C. Strain energy of random alloys: Wurtzite vs zinc blende

In a recent study, Van Schilfgaarde *et al.*[17] calculated the alloy formation enthalpies $\Delta H(x)$ for random $Ga_{0.5}In_{0.5}N$. They have chosen $A_8B_8N_{16}$ supercells to represent random wurtzite and zinc-blende alloys. In their 32-atom wurtzite supercell, the lattice vectors are two times larger than those of the primitive cell of the wurtzite structure, while they used a (111)-shaped symmetric unit cell for the 32-atom zinc-blende supercell. They relaxed the lattice parameters and cell-internal coordinates via a tight-binding method, and evaluated the formation enthalpies

$$\Delta H(x)=E_{\text{Ga}_{1-x}\text{In}_x\text{N}}-xE_{\text{InN}}-(1-x)E_{\text{GaN}} \tag{11}$$

at the relaxed geometry using the full-potential LMTO method. For $Ga_{0.5}In_{0.5}N$ they find $\Delta H^{32}_{\text{ZB}}=49$ meV/atom for the zinc-blende structure, and $\Delta H^{32}_{\text{WZ}}=69$ meV/atom for the wurtzite structure. The weighted energy difference between zinc-blende and wurtzite structures for the constituents,

$$\delta^{\text{ZB-WZ}}(x) = x[E^{\text{ZB}}_{\text{InN}} - E^{\text{WZ}}_{\text{InN}}] + (1-x)[E^{\text{ZB}}_{\text{GaN}} - E^{\text{WZ}}_{\text{GaN}}], \quad (12)$$

is $+11$ meV/atom at $x=0.5$,[25] while the formation energy difference $\Delta H_{\text{ZB}} - \Delta H_{\text{WZ}}$ is -20 meV/atom for $x=0.5$. Thus, their results suggest that for the 50%-50% alloy, the zinc-blende phase is *more stable* than the wurtzite phase (by around $20-11=9$ meV/atom), despite the fact that the end-point constituents prefer the wurtzite structure by 11 meV/atom.[25] To test whether such an alloy stabilized zinc-blende phase of $Ga_{0.5}In_{0.5}N$ can be obtained, we have computed, via the VFF approach $\Delta H^{32}_{\text{ZB}}$ and $\Delta H^{32}_{\text{WZ}}$ using the same 32-atom supercells as in Ref. 17. We found for $Ga_{0.5}In_{0.5}N$: $\Delta H^{32}_{\text{ZB}} = 36$ meV atom and $\Delta H^{32}_{\text{WZ}} = 55$ meV/atom. The VFF energy difference -19 meV/atom, and is thus similar to the LDA energy difference of -20 meV/atom. However, when we increase the supercell size to achieve better statistics by using the large supercells described in Sec. III, we find $\Delta H_{\text{ZB}} = +38.3$ meV/atom and $\Delta H_{\text{WZ}} = +38.2$ meV/atom. The formation energy due to strain is now nearly identical in random zinc-blende and wurtzite alloys. This is consistent with our observation shown in Fig. 3 that the bond distributions in zinc-blende alloys and wurtzite alloys are nearly identical. For the two other compositions investigated in this study, the wurtzite and the zinc-blende phases also have nearly identical formation energies: $\Delta H_{\text{WZ}} - \Delta H_{\text{ZB}} = -0.4$ meV/atom and -0.6 meV/atom, for $x=0.25$ and 0.75, respectively.

We thus conclude that the stabilization of about 9 meV/atom of the zinc-blende phase with respect to the wurtzite phase in random $Ga_{0.5}In_{0.5}N$ predicted by Ref. 17 is an artifact due to the small size and to the geometries of the supercells used in Ref. 17.

V. CONCLUSION

In summary, via an analytic model and large supercell (864–1024 atoms) VFF simulations, we investigated the nearest-neighbor bond-length distribution in tetrahedral (zinc-blende and wurtzite) and octahedral (rocksalt) $Ga_{1-x}In_xN$ alloys.

We found that, due to the rigidity of an octahedron (the bonds are either parallel or perpendicular to each other), the Ga-N (In-N) bond-length distribution in rocksalt alloys can be decomposed into a sum over two different peaked distributions: the first distribution corresponds to unrelaxed bonds while the second distribution corresponds to relaxed bonds. When both cations and anions are allowed to relax, these two peaks have a large width and overlap slightly, leading to a large spread of the nearest-neighbor distance distribution. On the other hand, the Ga-N (In-N) nearest-neighbor distribution in fully relaxed zinc-blende alloys can be decomposed into a sum over four peaks associated with different tetrahedral clusters. These four peaks are close to each other and have a much smaller width than those of the rocksalt alloys, leading to a sharp Ga-N (In-N) nearest-neighbor distribution and *looking like* single-peaked. Finally the wurtzite alloys exhibit bond-length distributions very similar to those of zinc-blende alloys, leading to a nearly identical strain energy in random zinc-blende and wurtzite alloys.

ACKNOWLEDGMENT

This work was supported by the U.S. Department of Energy, OER-BES-DMS Grant No. DE-AC36-83-CH10093.

[1] J. C. Mikkelsen and J. B. Boyce, Phys. Rev. Lett. **49**, 1412 (1982); Phys. Rev. B **28**, 7130 (1983); J. B. Boyce and J. C. Mikkelsen, *ibid.* **31**, 6903 (1985).
[2] A. Balzarotti, M. T. Czyzyk, A. Kiesiel, N. Motta, M. Podgorny, and M. Zimnal-Starnawska, Phys. Rev. B **30**, 2295 (1984).
[3] A. Balzarotti, N. Motta, A. Kiesiel, M. Zimnal-Starnawska, M. T. Czyzyk, and M. Podgorny, Phys. Rev. B **31**, 7526 (1985).
[4] C. K. Shih, W. E. Spicer, W. A. Harrison, and A. Sher, Phys. Rev. B **31**, 1139 (1985).
[5] J. L. Martins and A. Zunger, Phys. Rev. B **30**, 6217 (1984).
[6] A. Zunger and J. E. Jaffe, Phys. Rev. Lett. **51**, 662 (1983).
[7] Y. Cai and M. F. Thorpe, Phys. Rev. B **46**, 15 879 (1992).
[8] L. Bellaiche, S.-H. Wei, and A. Zunger, Phys. Rev. B **54**, 17 568 (1996).
[9] N. Motta, A. Balzarotti, P. Letardi, A. Kiesiel, M. T. Czyzyk, M. Zimnal-Starnawska, and M. Podgorny, Solid State Commun. **53**, 509 (1985).
[10] S.-H. Wei, L. G. Ferreira, and A. Zunger, Phys. Rev. B **41**, 8240 (1990).
[11] A. Silverman, A. Zunger, R. Kalish, and J. Adler, Phys. Rev. B **51**, 10 795 (1995); Europhys. Lett. **31**, 373 (1995).
[12] J. L. Martins and A. Zunger, Phys. Rev. Lett. **56**, 1400 (1986); J. Mater. Res. **1**, 523 (1986).
[13] A. Frenkel, E. A. Stern, A. Voronel, M. Qian, and M. Newville, Phys. Rev. Lett. **71**, 3485 (1993); Phys. Rev. B **49**, 11 662 (1994).
[14] A. Frenkel, E. A. Stern, A. Voronel, and S. M. Heald, Solid State Commun. **99**, 67 (1996).
[15] B. A. Bunker, Z. Wang, and Q. Islam, Ferroelectrics **120**, 23 (1991).
[16] Z. Wang and B. A. Bunker, Phys. Rev. B **46**, 11 277 (1992).
[17] M. Van Schilfgaarde, A. Sher, and A.-B. Chen, J. Cryst. Growth **178**, 8 (1997).
[18] P. N. Keating, Phys. Rev. **145**, 637 (1966).
[19] R. M. Martin, Phys. Rev. B **1**, 4005 (1970).
[20] K. Kim, W. R. L. Lambrecht, and B. Segall, Phys. Rev. B **53**, 16 310 (1996).
[21] These values differ somewhat from the ones given in Ref. 22 ($\alpha=81.09$ N/m and $\beta=12.16$ N/m in GaN, while $\alpha=63.58$ N/m and $\beta=8.05$ N/m in InN), which have been obtained by extrapolating the equation suggested in Ref. 19.
[22] I. Ho and G. B. Stringfellow, Appl. Phys. Lett. **69**, 2701 (1996).
[23] S.-H. Wei and A. Zunger, Appl. Phys. Lett. **69**, 2719 (1996).
[24] K. Kim, W. R. L. Lambrecht, and B. Segall (private communication).
[25] C. Yeh, Z. W. Lu, S. Froyen, and A. Zunger, Phys. Rev. B **46**, 10 086 (1992).